EEET ECOLOGICAL ENGINEERING & ENVIRONMENTAL TECHNOLOGY

Ecological Engineering & Environmental Technology, 25(12), 218–232
https://doi.org/10.12912/27197050/194127
ISSN 2299–8993, License CC-BY 4.0

Received: 2024.09.26
Accepted: 2024.10.15
Published: 2024.11.01

Co-Flow Jet Effects on the Aerodynamic Performance of National Renewable Energy Laboratory Aerofoils with Different Thicknesses for Wind Turbine Applications

Aljunayd Mohamed Aloukili[1,2*], Mohamed Elsakka[3], Mostafa Ali Mohamed [2], Mohamed Elfaisal Elrefaie[2]

[1] Department of Mechanical Engineering, University of Derna, Derna, Libya
[2] Department of Mechanical Engineering, Al Azhar University, Cairo, Egypt
[3] Department of Mechanical Power Engineering, Port Said University, Port Said, Egypt
* Corresponding author's e-mail: aljonaid.mohammed@uod.edu.ly

ABSTRACT

The design of wind turbines has been continually evolving to enhance aerodynamic efficiency, which is crucial for improving energy conversion and reducing operational costs. One promising technique is the application of the Co-Flow Jet (CFJ) method, which utilizes simultaneous blowing and suction to augment aerofoil performance. Despite its potential benefits, the relationship between aerofoil thickness and the resulting improvements in lift and drag coefficients has not been thoroughly explored, especially for the National Renewable Energy Laboratory (NREL) aerofoils commonly used in wind turbine applications. This study utilizes computational fluid dynamics (CFD) simulations in order to investigate the aerodynamic efficiency improvements of the NREL S826, NREL S825, and NREL S818 aerofoils through the application of the CFJ technique. Various configurations with different blowing (B) and suction (S) configurations were tested, including 0.08B-0.7S, 0.08B-0.8S, 0.1B-0.7S, and 0.2B-0.7S configurations. The results demonstrate that the S826-0.2B-0.7S, S825-0.2B-0.7S, and S818-0.08B-0.7S configurations yield the most significant enhancements at a common momentum coefficient (C_m) of 0.08. Specifically, there were increases in lift coefficients by about 51.1%, 66.38%, and 109%, and improvements in lift-to-drag ratios by about 11.5%, 14.38%, and 146.18% for the S826-0.2B-0.7S, S825-0.2B-0.7S and S818-0.08B-0.7S configurations, respectively.

Keywords: Co-Flow Jet, NREL (S826-S825-S818) aerofoil, lift and drag coefficient, lift to drag ratio, wind turbine blade.

INTRODUCTION

Given the increasing prominence of environmental pollution and energy shortages, the global focus has shifted towards the development and exploitation of new energy sources. Renewable energy will have a significant impact on enhancing the ecological environment, optimizing the energy composition, and driving sustainable social and economic progress. Wind power is recognized as the most developed, extensive, and promising form of energy generation among emerging technologies (Yuan et al., 2023). Wind turbines are widely utilized devices designed to capture the kinetic energy of wind and convert it into usable electrical power. Wind turbines can be classified into two main categories. These include horizontal-axis wind turbines (HAWT) and vertical-axis wind turbines (VAWT). Among VAWTs, there are two distinct designs: the Savonius design, which is primarily considered as a drag-driven device, and Darrieus design that relies on streamlined aerofoils and is primarily driven by lift forces. The performance of HAWT and Darrieus VAWT is heavily dependent on the aerodynamics of their aerofoils (Elsakka et al., 2021, Tayebi et al., 2024) To enhance the overall performance of these turbines, it is crucial in improving the lift coefficient as well as the lift-to-drag ratio of the aerofoil. Achieving a higher lift coefficient also involves delaying flow separation at higher angles of attack. Several configurations have been developed to increase lift while addressing and mitigating flow separation. One of the strategies is the use of CFJ which was proposed by Prandtl (Yousefi et al., 2014) CFJ is a flow control technique that maintains zero net mass flux. It includes an injection slot positioned at near the leading edge and a suction slot located at the trailing edge on the aerofoil's suction side (Liu et al., 2022) The primary concept underlying jet blowing and suction is to introduce an external momentum to the flow stream over the aerofoil, thereby altering the boundary layer characteristics. This additional momentum enhances the flow stream's ability to adhere to the aerofoil wall for a longer duration, thereby increasing the stall angle. Consequently, the aerofoil's capacity to generate higher lift force values is augmented, leading to higher power coefficients of wind turbines (Wang et al., 2022; Abbasi et al., 2022). The NACA0012 aerofoiled blade was subjected to an experimental investigation to examine the impact of perpendicular blowing and suction jet hole geometry at Reynolds number (Re) equal to 1×10^5 while maintaining a turbulence intensity below 0.5%. The perforations were positioned at intervals of 0.2 and 0.3 along the length of the cord for the purpose of blowing. The inner diameter of each hole was 1 mm, and the row width accounted for 0.93 of the span length. The jet intensity can be characterized by altering the momentum coefficient, C_m (Wang et al., 2022)

Xu et al., (2020) explored the use of co-flow jet active flow control on wind turbine aerofoils, focusing on the effects of different variables such as the size and location of injection and suction slots, as well as injection total pressure. The study found that the optimal configuration achieved a 42.3% boost in the maximum lift coefficient. However, the limited range of parameter values, with only three options tested for each variable, restricted the study's scope. Additionally, the enhanced configuration did not improve the lift-to-drag ratio in contrast with the baseline case.

Sun et al. (2019) conducted a computational study to improve the performance of a vertical axis wind turbine based on NACA 0015 aerofoil by integrating a co-flow jet. The research revealed that placing the suction ports at 80% from the leading edge of the aerofoil and positioning the blowing at 3% of the chord were effective in controlling flow separation, leading to improved aerofoil efficiency. At low tip speed ratio, the power coefficient of the turbine increased by about 170%. This study emphasized the importance of precise CFJ injection placement in boosting the performance of vertical-axis wind turbines.

Balaji et al. (2020) conducted an empirical study on the NACA 6415 aerofoil using a convergent nozzle. The findings indicated a 5-degree enhancement in the stalling angle of attack when compared to a standard aerofoil. Additionally, the overall lift coefficient is increased by 43% despite only a minimal rise in lift-induced drag.

Zhang et al. (2021) introduced a method for adjusting the jet momentum coefficient in an adaptive manner. They employed the CFJ on the S809 aerofoil and evaluated their approach using the PHASE VI wind turbine blade. They utilized the blade element-moment (BEM) theory for the performance assessment. It was observed that the power coefficient of the turbine based on the CFJ blade is improved by about 226.7% for a tip speed ratio of 1.52.

Arunraj et al. (2019) carried out an experimental study on a Modified CFJ (MVCJ) aerofoil, comparing its performance to that of a standard aerofoil. The modification involved incorporating a convergent-divergent (CD) nozzle at the injection slot to lessen the load on the pump. The results showed a 43% increase in the lift coefficient for the modified aerofoil compared to the unmodified version.

Xu et al.,(2021) utilized CFJ on the S809 wind turbine aerofoil and successfully obtained an optimized configuration of the CFJ-S809 aerofoil. This optimization resulted in a substantial enhancement in both the lift coefficient (C_L) and the aerodynamic efficiency lift to drag ratio (C_L/C_D) that would lead to an enhancement of the wind turbine power output by about 12.3%.

Ren et al. (2020) performed a computational study on the NACA 6421 aerofoil, utilizing both the CFJ technique and the propeller actuator method in two-dimensional and three-dimensional simulations. The outcomes were benchmarked against the baseline aerofoil under normal cruise conditions. Furthermore, it is revealed that the 2D CFJ implementation significantly enhances cruise efficiency, with a 46.86% improvement for the CFJ aerofoil and about 21% increase for the propeller actuator configuration. However, in 3D simulations, the aerodynamic efficiency of the propeller actuator setup improved by 7.11% over the baseline, while productivity efficiency saw an 11.17% boost.

Boling et al. (2020) conducted a detailed conceptual design analysis on a complete aircraft using a NACA 6415 wing. They did a numerical analysis at a Mach number (Ma) of 0.6 under cruising conditions. Empirical evidence has demonstrated that the novel conceptual design successfully attained a 14.6% enhancement in aerodynamic efficiency, as indicated by a lift coefficient of 0.812. Additionally, it was observed that the power required for hovering is decreased by 21.7%.

Zha et al. (2007) conducted a separate study on a CFJ aerofoil, where they carried out wind tunnel tests on a NACA 0025 aerofoil and its modification with CFJ. The experiments were performed at a Reynolds number of 380,000 and a Mach number of 0.11, covering various angles of attack and the momentum coefficients between 0.1 and 0.3. Moreover, the results demonstrated that the CFJ-enhanced aerofoil produced a substantial lift increase, ranging from 113% to 220%. The stall margin exhibited a notable gain of 53%, going from 100% to 153%, while the drag coefficient (C_D) experienced a reduction of 97%, dropping from 127% to 30%. Consequently, this led to a boost in thrust. The superiority of the CFJ aerofoil in terms of aerodynamic performance, when compared to the baseline aerofoil, is readily apparent. Table 1 provides an overview of past research on the effects of CFJ on aerofoil aerodynamics, highlighting the types of studies, aerofoil models used, Reynolds numbers (Re), slot designs, and the momentum coefficients for both blowing ($C_{m,b}$) and suction ($C_{m,s}$). It also compares the lift (C_L) and drag (C_D) outcomes, offering a comparison of how various CFJ setups affect aerodynamic performance and summarizing the advantages and drawbacks found in different studies.

Despite extensive efforts to optimize CFJ technology through various designs that modify the dimensions and locations of blowing and suction ports for different aerofoils, the relationship between aerofoil thickness and the resulting improvements in lift and drag coefficients remains underexplored. This study addresses this gap by investigating CFJ enhancements for three NREL aerofoils with varying thicknesses: NREL S826, NREL S825, and NREL S818 which have been implemented in several wind turbines (Malcolm et al., 2006, Li et al., 2021; Ibrahim et al., 2024). The primary objectives are to identify the most effective positions for the suction and blowing jet

Table 1. Summary of previous studies on the effect of CFJ on the aerodynamic performance of an aerofoil

Author	Type of investigation	Aerofoil	Re	Slot type	Geometry	$C_{m,b}$	$C_{m,s}$	C_L	C_D
Goodarzi et al., 2012	Numerical simulation	NACA0012	5 x 10^5	Perpendicular	X/C)s = 0.1 $H)_S$ = 2.5%C	0	0.025	45%	-29%
Yousefi et al., 2014	Numerical	NACA0012	5 x 10^5	Perpendicular	$X/C)_b$ = 0.8 H = 4%C	A = 0.5	0	-23%	-16%
				Tangential	$X/C)_b$ = 0.8 H = 4%C	A = 0.5	0	7%	-7%
				Perpendicular	$X/C)_S$ = 0.1 H = 2.5%C	0	A = 0.5	75%	-56%
Müller-Vahl et al., 2015	Experimental	NACA0018	2.5 x 10^5	Tilted by Θ = 20°	$X/C)_b$ = 0.05	0.05	0	65%	___
Xu et al., 2016	Numerical simulation	NRELS809	10^6	Tilted by Θ = 30°	$X/C)_b$ = 0.06 $H)_b$ = 0.65%C X/C)s = 0.8 $H)_S$ = 1.38%C	0.12	0.12	51.1%	-78%
James et al., 2018	Numerical	NACA0012	5 x 10^5	Secondary flow	$X/C)_b$ = 0.6	A = 0.2	0	3.97%	___
		LA203A			$X/C)_b$ = 0.6	A = 0.2	0	0.72%	___
Wang et al., 2022	Experimental	NACA0012	1 x 10^5	Perpendicular	$X/C)_b$ = 0.2	0.104	0	18.4%	Negl.
					$X/C)_b$ = 0.2 X/C)s = 0.6	0.104	0.058	Negl.	Negl.
Zhu et al., 2022	Experimental	NACA0012	1 x 10^5	Perpendicular	$X/C)_b$ = 0.2,0.3 $X/C)_S$ = 0.6	0.026 to 0.418	0.026 to 0.418	18.4%	Negl.

ports and to clarify the relationship between aerofoil thickness and potential enhancements in lift, drag, and lift-to-drag coefficient values.

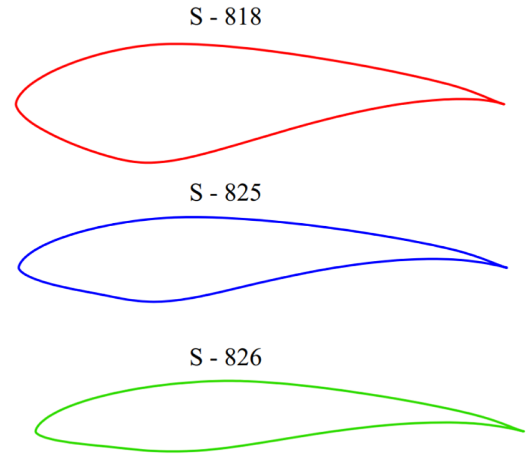

Figure 1. The geometry of the baseline NREL S818, NREL S825, and NREL S826 without the blowing and suction ports

NUMERICAL MODELLING

Computational fluid dynamics (CFD) is widely recognized as an effective tool in the development and testing of designs and concepts. CFD accelerates the transition of designs into practical applications, often more rapidly and cost-effectively than traditional experimental methods. Although experimental approaches can provide the most accurate results in certain cases, well-executed CFD simulations can yield highly reliable results that closely approximate experimental findings. CFD has been utilized for the current investigation. The double-precision pressure-based version of Ansys Fluent solver has been utilized to analyse the flow around NREL S826, NREL S825 and NREL S818 aerofoils, utilizing a simultaneous blowing and suction CFJ technique. Structured mesh topologies have been employed due to their computational efficiency, numerical accuracy, and robustness. A total of 1.000 iterations are performed in each simulation and this has been found to be sufficient to ensure that the residuals are lower than 1×10^{-5}.

The RANS-based approach has been utilized that provides a finite element solution method using the governing equations for mass, energy, and momentum. The study incorporated the SST k-ω turbulence model, which is based on dissipation rate and turbulent kinetic energy, with a turbulence intensity of 5%.

Figure 1 presents the baseline geometries of the NREL S818, NREL S825, and NREL S826 aerofoils, emphasizing the differences in their thicknesses. Various geometric modifications were considered for these aerofoils, including the incorporation of blowing and suction ports. The blowing port was set at a width of 2% of the chord length (C). On the other hand, the suction port was 3% of the chord length. Both ports were fixed at specific tilt angles, with the blowing port at 35° and the suction port at 145° relative to the x-axis as illustrated in Figure 2. This study evaluates the impact of different port positions and

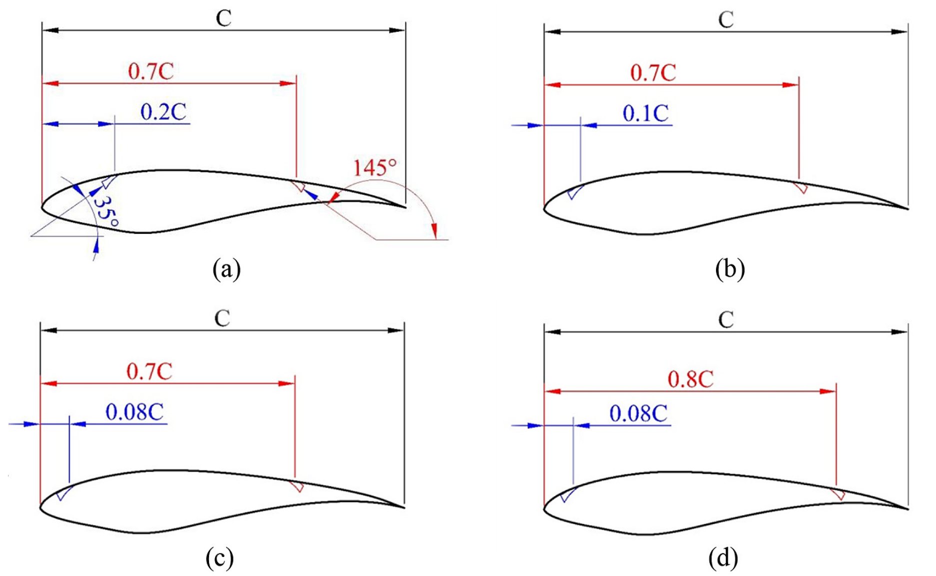

Figure 2. Various CFJ configurations over a NREL S825 aerofoil including (a) S825 0.2B-0.7S (b) S825 0.1B-0.7S, (c) S825 0.08B-0.7S and (d) S825 0.08B-0.8S

momentum coefficients on the aerodynamic characteristics of the NREL S826, NREL S825, and NREL S818 aerofoils. The selected blowing port positions are at 0.08 C, 0.1 C, and 0.2 C, while the suction port positions are at 0.7 C and 0.8 C. A wide range of momentum coefficients, C_m, is explored, including values of 0.05, 0.08, 0.16, and 0.2. A coding system has been developed for aerofoils with suction and blowing ports to facilitate the identification of port positions. For example, in the code S825-0.2B-0.7S, "S825" represents the aerofoil section, "0.2B" indicates the blowing port located at 0.2 of the chord length, and "0.7S" indicates the suction port located at 0.7 of the chord length, measured from the leading edge (Fig. 2). Figure 2 also displays the different sets of CFJ geometrical configurations considered for the NREL S825 aerofoil. The same geometrical configurations are applied to the NREL S818 and NREL S826 aerofoils.

The CFD domain used in the current study extends 10 chord lengths upstream from the aerofoil and 20 chord lengths downstream, as shown in Figure 3. A structured mesh topology has been applied to both the baseline aerofoils and those with suction and blowing ports. Examples of the constructed mesh are depicted in Figure 4 for the NREL S825 and NREL S818 aerofoils, as well as for the cases S825-0.2B-0.7S and S818-0.2B-0.7S.

The mesh is constructed using ANSYS Meshing software, with careful attention to standard

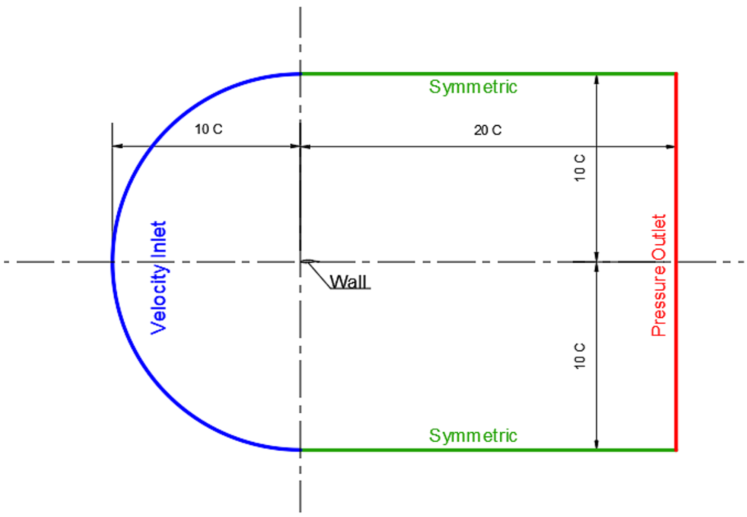

Figure 3. The computational domain used in the current case study, extending 10 times the chord length upstream from the leading edge, and 20 times the chord length from the trailing edge

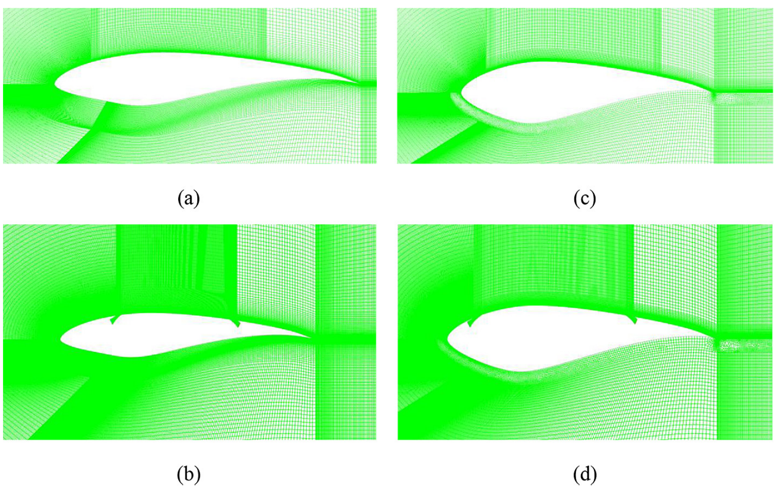

Figure 4. Structured mesh topology generated for the CFD simulation of (a) the baseline NREL S825 design, (b) the CFJ-augmented S825-0.2B-0.7S aerofoil, (c) the baseline NREL S818 design, and (d) the CFJ-augmented S818-0.08B-0.7S aerofoil

meshing principles to ensure precise and accurate results. The mesh depicted in Figure 4 has a higher density of elements near the aerofoil surface to capture the rapid and complex changes in fluid flow parameters within the boundary layer. The simulation is conducted at a Reynolds number (Re) of 6×10^5, employing simultaneous blowing and suction with an equal momentum coefficient (C_m) for both processes. The equation for C_m is:

$$C_m = \frac{\dot{m}_j V_j}{0.5\,\rho U_\infty^2 S} \quad (1)$$

where: C_m – momentum coefficient, Vj – jet velocity, ρ – air density at normal atmospheric conditions, m_j – jet mass flow rate, U_∞ – ambient air velocity, S – the aerofoil span side area.

While the blowing and suction flow rates remain consistent across each case, the momentum coefficient (C_m) values vary from 0.05 to 0.2, corresponding to flow rates ranging from 0.24 to 0.49 kg/s. Specifically, the C_m values are set at 0.05, 0.08, 0.16, and 0.2, with corresponding flow rates of 0.24, 0.31, 0.43, and 0.49, respectively. A mass flow inlet boundary condition is applied at the entrance of the blowing nozzle while a mass flow rate outlet boundary condition is imposed to determine the mass exiting the suction port.

RESULTS AND DISCUSSION

The primary goal of the blowing and suction CFJ technique, as indicated by the literature review, is to mitigate the separation phenomena that hinder the improvement of the aerodynamic properties of the aerofoil. An aerofoil is considered to have superior aerodynamic properties when it achieves a high lift coefficient (C_L) while simultaneously maintaining a low drag coefficient (C_D), or even obtaining even lower C_D values. This can be achieved by producing conditions in which the airflow can impinge on the aerofoil profile at high angles of attack (α) without separating from the aerofoil surface. Such conditions can be created using the (CFJ) technique, as observed. The key design parameters that are considered in this study include the location of the blowing and suction ports along the chord length of the aerofoil the location of blowing port with respect to the chord length $(X/C)_B$ and the location of suction port with respect to the chord length $(X/C)_S$, the momentum coefficient (C_m), and the aerofoil thickness.

Validation

To ensure the reliability and realism of the CFD-generated results, the numerical predictions are validated against the experimental data from (Barti et al., 2019) for the base configuration of the NREL S826 aerofoil. Figure 5 demonstrates a good agreement between the CFD predictions and the detailed experimental data (Barti et al., 2019) for both the lift and drag coefficients of this aerofoil. Therefore, the same CFD methodology can be utilized for the different geometrical configurations in the current case study in order to ensure the reliability of the obtained results.

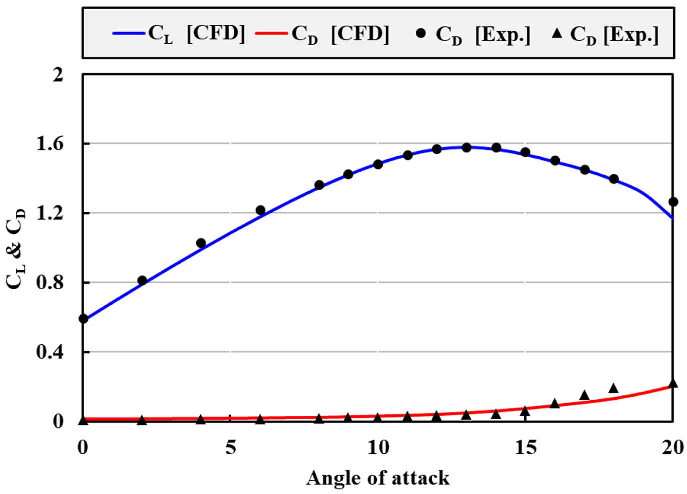

Figure 5. Comparison between CFD predictions and experimental results by (Barti et al., 2019) for both lift and drag coefficients of the NREL S826 aerofoil

The effect of both blowing and suction ports position and momentum coefficient variation over the aerodynamic performance of the NREL S825, NREL S818 and NREL S826

For NREL S825 aerofoil, the simulation is initially performed at a fixed position for the blowing and suction ports particularly for the S825-0.2B-0.7S configuration while varying the values of C_m from 0 to 0.2. Figure 6 depicts the variation of lift and drag coefficients over a range of angle of attack considering different momentum coefficients considering the S825-0.2B-0.7S configuration. At first glance, the prevailing impression is that the higher the value of C_m, the higher the value of C_L, with a slight change in the value of C_D at low and moderate angles of attack. Stall delay is also a clear effect that appears over the S825-0.2B-0.7S configuration for all considered C_m values.

It can be observed that, at a particular angle of attack, the lift coefficient (C_L) witnesses an enhancement with a minor change in the value of drag coefficient (C_D), achieving high stall delay values when applying the simultaneous blowing and suction CFJ technique. This mainly is due to the intentionally generated vortexes that exchange their momentum with the main wind streamlines. This is found to affect the aerofoil aerodynamics throughout the angle of attack range. At low values of the angle of attack, the excess momentum added to the mainstream increases the generated lift coefficient as the resulting lift force increases. For a bigger attack angle (α), where stall normally occurs at the base condition, the excess applied momentum forces the mainstream to be kept attached to the aerofoil surface.

The influence of the simultaneous blowing and suction CFJ technique on the pressure distribution and flow pattern around the S825-0.2B-0.7S aerofoil, when subjected to varying momentum coefficient (C_m) values at the reference stall angle of attack, is illustrated in Figure 7. The reference stall angle value corresponds to the stall angle observed without the application of CFJ and

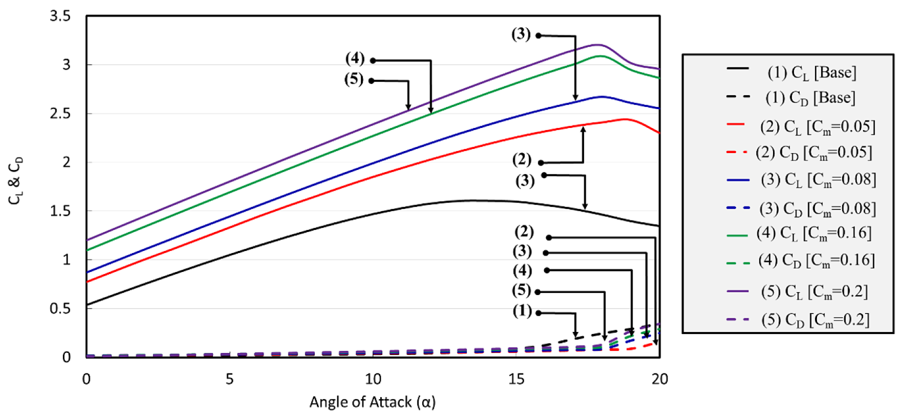

Figure 6. Variation of lift and drag coefficients over a range of angle of attack under the influence of momentum coefficient for the S825-0.2B-0.7S configuration

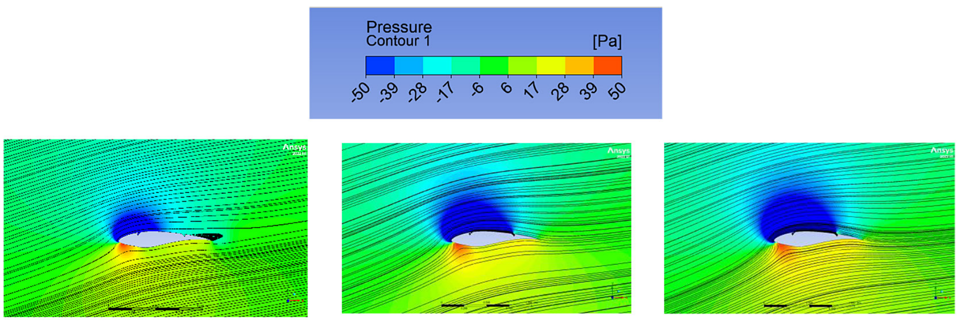

(a) (b) (c)

Figure 7. The impact of applying (a) C_m = 0 (base case), (b) C_m = 0.08, and (c) C_m = 0.2 on the pressure distribution and flow pattern around the S825-0.2B-0.7S configuration at the reference onset stall angle of attack AOA (angle of attack), 14°

is considered 14° for S825-0.2B-0.7S aerofoil. As depicted in Figure 7a, Figure 7b, and Figure 7c, the application of simultaneous blowing and suction CFJ at the reference stall angle of attack effectively results in a more uniform velocity distribution across the aerofoil and eliminates the flow separation near the trailing edge. Introducing the CFJ technique is observed to increase the extent of the negative suction pressure region that is adjacent to the aerofoil suction side. As a result, the aerofoil demonstrates more stable operation and achieves a higher lift coefficient, though this is accompanied by an increase in the drag coefficient at the reference stall angle, as shown in Figure 6.

It is observed that even at low C_m values, the CFJ technique significantly enhances the lift coefficient while causing only a modest increase in the drag coefficient. However, any increase in drag force can significantly impact overall aerofoil performance, particularly in wind turbine applications. To more accurately assess the effect of the CFJ technique on overall aerofoil performance, it is essential to analyse the lift-to-drag ratio. Figure 8 illustrates the variety of the lift-to-drag ratio over a range of different angles of attack concerning various C_m values. Figure 9 presents a logarithmic representation of the lift, drag coefficient and lift-to-drag ratio that occurs at the reference stall angle value of attack for each configuration for various CFJ configurations. It should be noted that, due to the logarithmic scale, the observed improvements may appear less pronounced than they actually are. As can be observed, the S825-0.2B-0.7S configuration can be

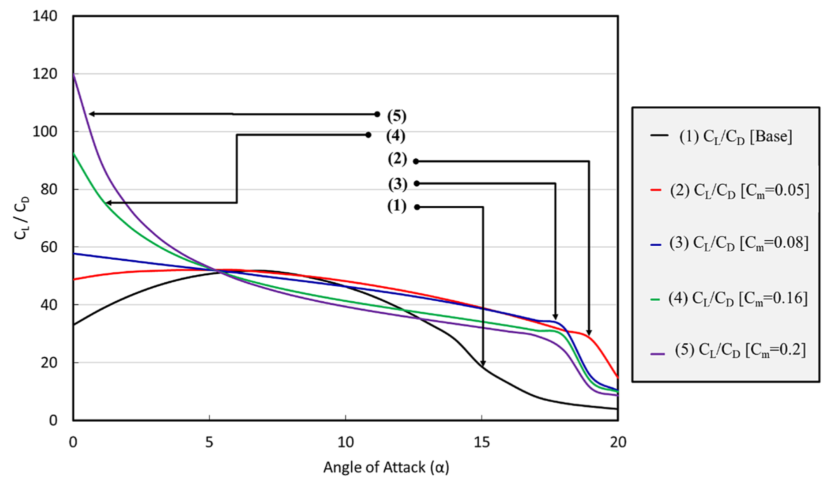

Figure 8. The variation in lift-to-drag ratio across a range of different angles of attack under the influence of momentum coefficient for the S825-0.2B-0.7S configuration

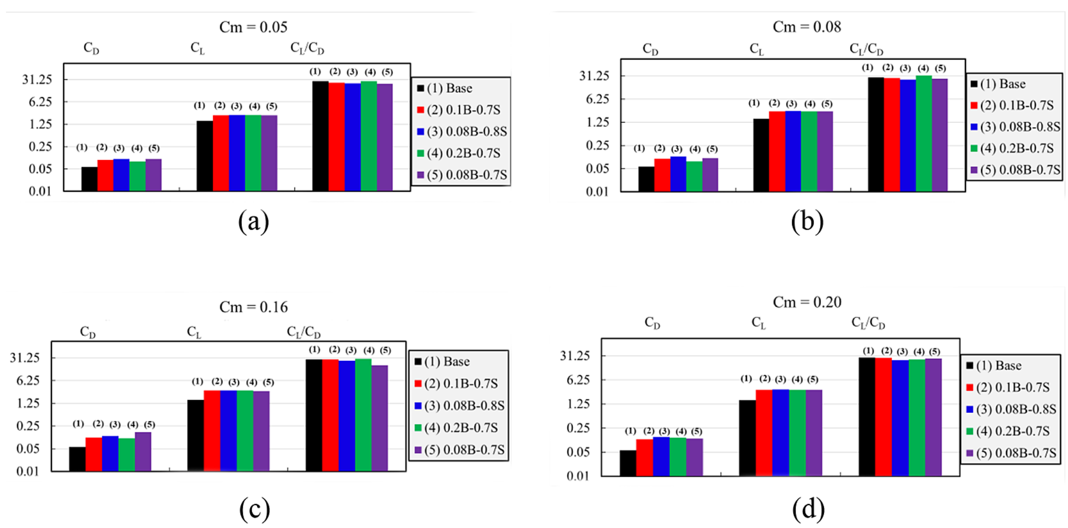

Figure 9. Lift, drag, and lift-to-drag coefficients for various CFJ configurations applied to the NREL S825 aerofoil at the onset stall angle of attack

considered the best design among the presented configurations for the aerofoil NREL S825 when applying a C_m = 0.08, this configuration managed to increase the lift coefficient value with the lowest possible increase in drag coefficient value compared to the other NREL S825 configurations at various C_m values which allows it to give the highest aerodynamic performance enhancement with the CFJ technique been applied.

For the S825-0.2B-0.7S configuration at the reference onset stall angle, the application of the CFJ technique with a C_m of 0.05 leads to a 51.63% increase in lift coefficient, a 51.52% rise in drag coefficient, and a slight 0.073% improvement in lift-to-drag ratio. When Cm is increased to 0.08, the lift coefficient sees a 66.38% boost, the drag coefficient grows by 45.45%, and lift-to-drag ratio improves by 14.38%. Considering C_m of 0.16, the lift coefficient increases by 92.4%, the drag coefficient rises by 85.26%, and the lift-to-drag ratio experiences a moderate gain of 3.855%. However, at a C_m of 0.20, while the lift coefficient further increases by 102.92%, the drag coefficient jumps by 130.86%, resulting in a decrease in the lift-to-drag ratio by 3.851%.

The simulation for the NREL S818 followed the same methodology as that used for the NREL S825. Figure 10 shows the variations in lift and drag coefficients as a function of the angle of attack for the S818-0.08B-0.7S configuration. The results reveal that consistent with the behaviour observed in the NREL S825 configuration, an increase in C_m generally enhances the lift coefficient, particularly at low to moderate angles of attack. However, the drag coefficient shows only minor variations at angles of attack lower than the onset stall angle of attack. Furthermore, the application of the CFJ technique leads to a noticeable delay in the stall across the S818-0.08B-0.7S configuration for most C_m values. This mainly is due to the intentionally generated vortexes working to exchange their momentum with the main wind streamlines which leads to the following results, at low values of attack angle (α) the excess momentum added to the mainstream increases the generated lift coefficient as the resulting lift force increase. For a bigger attack angle (α), where stall normally occurs at the reference stall angle value of attack, the excess applied momentum forces the mainstream to be kept attached to the aerofoil surface.

The influence of the simultaneous blowing and suction CFJ technique on the pressure distribution and flow pattern around S818-0.08B-0.7S configuration, with different C_m values applied at the base onset stall angle of attack, is illustrated in Figure 11. As the C_m increases, the low-pressure region over the suction side of the aerofoil increases and hence the lift coefficient increases.

The investigation of the performance of the provided S818 aerofoil confirms the conclusion that applying the minimal C_m values can enhance the lift coefficient as well as the overall aerofoil performance. However, the drag coefficient slightly increases with increasing the C_m. Figure 12 illustrates the variety of the lift-to-drag ratio at different angles of attack for various C_m values. It is clear that the CFJ enhances the lift-to-drag ratio is enhanced especially when the angle of attack is larger than the onset angle of attack. Figure 13 presents the lift and drag coefficient and the lift-to-drag ratio that occur for various CFJ configurations applied for NREL S818 aerofoil at the onset stall

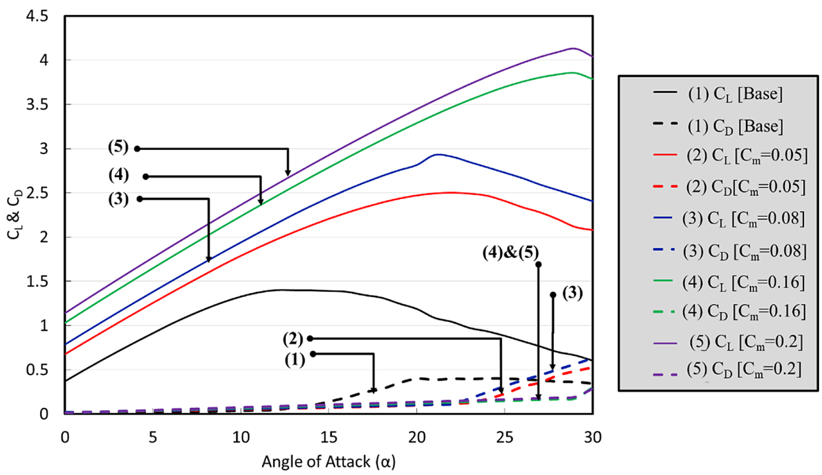

Figure 10. Variation of lift and drag coefficients with angle of attack under the influence of momentum coefficient for the S818-0.08B-0.7S configuration

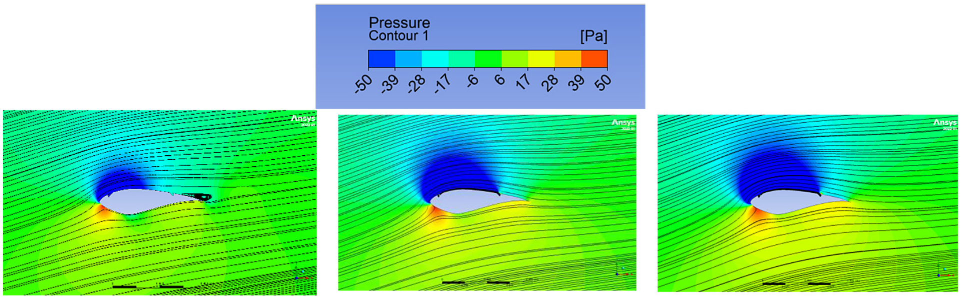

(a) (b) (c)

Figure 11. The effect of applying (a) C_m = 0 (base case), (b) C_m = 0.08, and (c) C_m = 0.2 on the aerodynamic field of the S818-0.08B-0.7S configuration at the reference onset stall angle of attack AOA, 12º

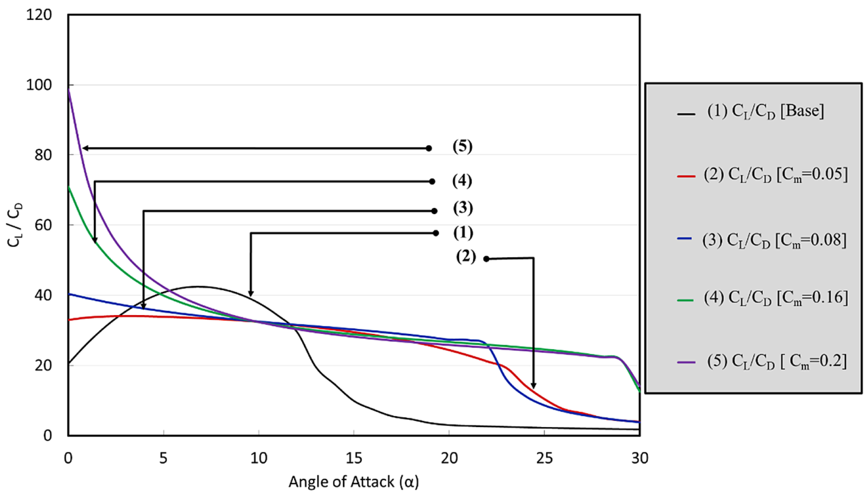

Figure 12. The variation of lift-to-drag coefficients over a range of angle of attack value under the effect of momentum coefficient for the S818-0.08B-0.7S configuration

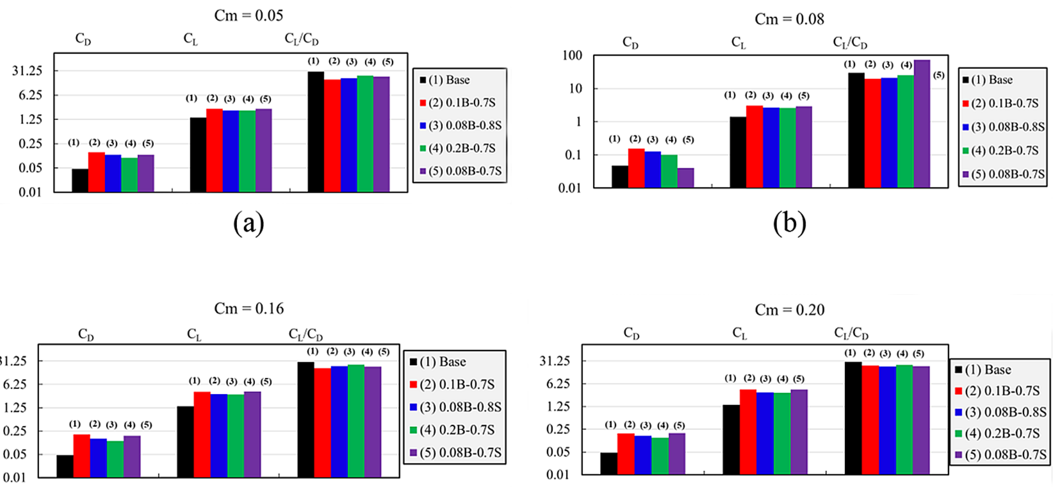

(a) (b) (c) (d)

Figure 13. Changes in lift, drag, and lift-to-drag coefficients for various CFJ configurations applied to the NREL S818 aerofoil at the onset stall angle of attack

angle of attack. As can be observed that the S818-0.08B-0.7S configuration can be considered the best design among the presented configurations for the aerofoil NREL S818 at a C_m = 0.08. this configuration assists in increasing the lift coefficient value with a minimal drag coefficient value compared to the other NREL S818 configurations at various C_m values which allows it to give the highest aerodynamic performance enhancement with the CFJ technique.

For the S818-0.08B-0.7S configuration at the onset stall angle, the application of the CFJ technique with $C_m = 0.05$ results in a 78.61% rise in the lift coefficient, a 150.28% of increase in the drag coefficient, and a 28.63% of reduction in the lift-to-drag ratio. When C_m is increased to 0.08, lift coefficient improves by 109%, drag coefficient decreases by 15.1%, and the lift-to-drag ratio possess significant increase of 146.18%. At $C_m = 0.16$, the lift coefficient experiences a 175.2% rise, while the drag coefficient increases by 277.18%, leading to a 27.03% drop in the lift-to-drag ratio. Finally, with C_m set at 0.20, the lift coefficient climbs by 194.83%, the drag coefficient by 304.74%, and the lift-to-drag ratio has been decreased by 27.16%.

The simulation for the NREL S826 was conducted using the same methodology applied to the NREL S825 and S818. Figure 14 depicts the variation in lift and drag coefficients as the angle of attack changes under different C_m for the S826-0.2B-0.7S configuration. The results indicate a consistent trend: higher Cm values lead to an increase in the lift coefficient, while the drag coefficient exhibits minimal change at low to moderate angles of attack. Additionally, stall delay is a recurring effect observed in theS826-0.2B-0.7S configuration for most applied C_m values. These results suggest that the CFJ technique induces similar aerodynamic effects across the tested NREL S-family aerofoils.

Figure 15 depicts the influence of the simultaneous blowing and suction CFJ technique on the pressure distribution and flow pattern around the S826-0.2B-0.7S configuration for different C_m values at the reference onset stall angle of attack. It can be observed from Figure 15 that the implementation of simultaneous blowing and suction CFJ increases the size of both the high-pressure region around the pressure side and the

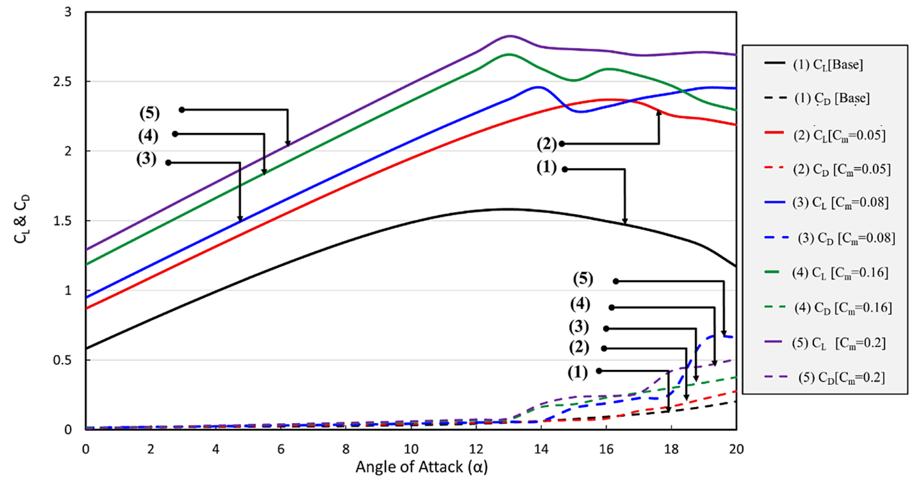

Figure 14. Variation of lift and drag coefficients with angle of attack under the influence of momentum coefficient for the S826-0.2B-0.7S configuration

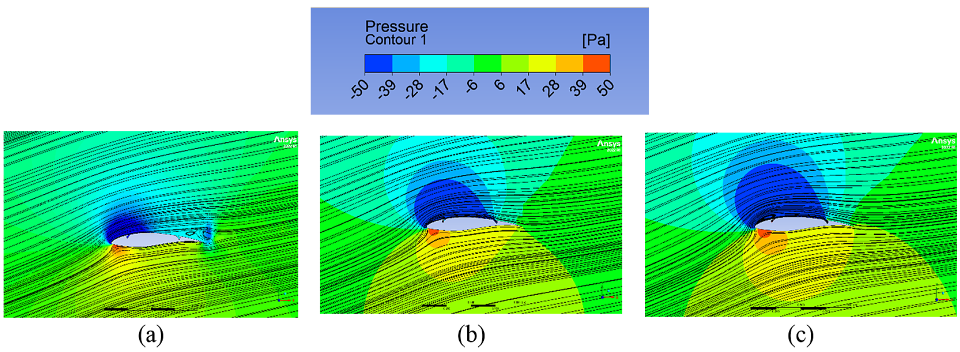

Figure 15. Effect of applying (a) $C_m = 0$ (base case), (b) $C_m = 0.08$, and (c) $C_m = 0.2$ on the aerodynamic field of the S826-0.2B-0.7S configuration at the reference onset stall angle of attack AOA, 15°

low-pressure region around the suction side. This increases the lift coefficient with the increase in C_m. Furthermore, the CFJ successfully eliminate the trailing edge separation that already occurs in the baseline aerofoil without CFJ.

Figure 16 illustrates the variation in the lift-to-drag ratio at different angles of attack for various C_m values. Figure 17 details the changes in lift, drag, and lift-to-drag ratios across different CFJ configurations applied to the NREL S826 aerofoil. The data suggest that the S826-0.2B-0.7S configuration possesses a favourable lift coefficient with a low drag coefficient while achieving the highest lift-to-drag ratio hence the S826-0.2B-0.7S configuration is considered the optimal design among the configurations tested for the NREL S826 aerofoil when C_m = 0.08 is applied. This configuration achieves the most significant increase in lift coefficient while minimizing drag, resulting in the highest aerodynamic performance enhancement with the CFJ technique.

When comparing the aerodynamic coefficients at the onset stall angle of attack with and without the CFJ technique, using a C_m of 0.05 leads to a roughly 50% rise in lift coefficient and about a 60% increase in drag coefficient while achieving a 6% decrease in lift-to-drag ratio compared to the configuration without CFJ. At C_m = 0.08, the S825-0.2B-0.7S configuration shows a 55% enhancement in lift coefficient and a 24% increase in drag coefficient while achieving a 25% improvement in lift-to-drag ratio. Increasing C_m to 0.16 results in a 64% gain in lift coefficient. In addition, a 223% rise in the drag coefficient is achieved along with a 49% drop in the lift-to-drag ratio. With C_m = 0.20, the lift coefficient increases by 72%, the drag coefficient by 380%, and the lift-to-drag ratio decreases by 64% compared to the non-CFJ case.

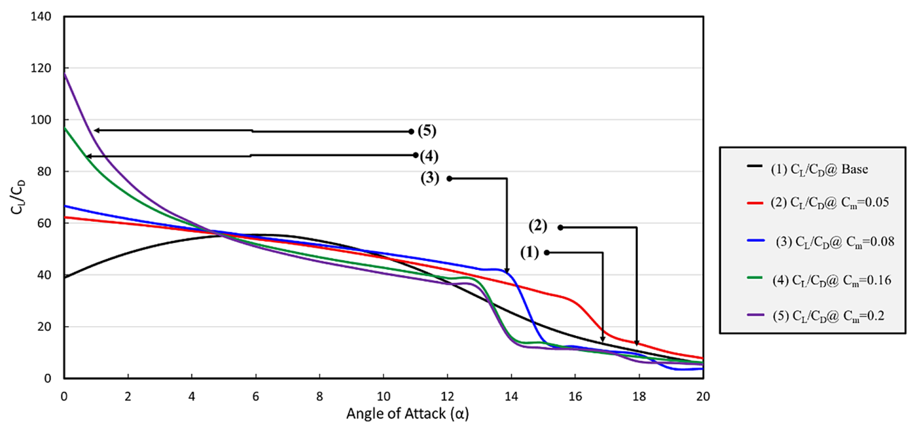

Figure 16. Variation of lift-to-drag ratio over a range of angle of attack under the influence of momentum coefficient for the S826-0.2B-0.7S model

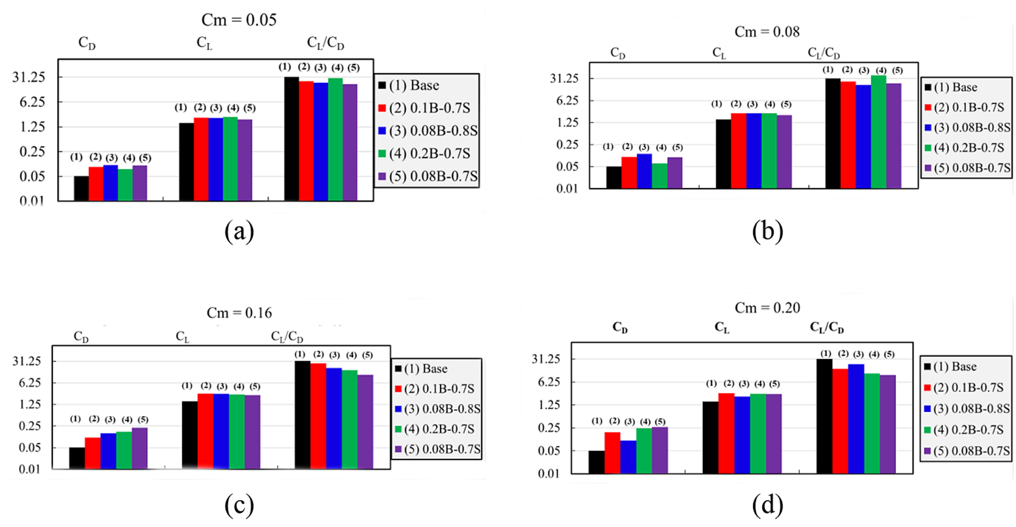

Figure 17. Changes in the lift, the drag, and lift-to-drag coefficients for various CFJ configurations applied to the NREL S826 aerofoil at the onset stall angle of attack

The performance analysis of the S826 configurations supports the conclusion that applying minimal C_m values can improve the lift coefficient and overall aerofoil performance. However, C_m values below 0.08 yield negligible enhancements, indicating that $C_m = 0.08$ is likely the optimal value for application across the NREL S-family.

The effect of aerofoil thickness on performance and its influence on the effectiveness of the CFJ technique

Figure 18 illustrates the performance of the S826, S825, and S818 aerofoils, each with notably different profile thicknesses. As previously shown in Figure 1, the differences between the S826 and S825 are primarily due to increased surface curvature on the pressure side, while both profiles share the same geometry on the suction side. Hence, the performance of S826 and S825 is relatively similar. Greater surface curvature on an aerofoil generally accelerates the flow, leading to increased momentum. However, this benefit is limited; at lower angles of attack, excessive curvature can cause the boundary layer to reach its maximum velocity and minimum pressure prematurely, leading to a loss of momentum and flow separation from the aerofoil surface. Also, greater thickness would result in larger drag. As illustrated in Figure 18 and considering the aforementioned phenomenon, thicker blade profiles tend to experience flow separation at lower angles of attack. Beyond a certain thickness, unfavourable conditions arise due to the formation of high-velocity vortices, which increase drag and reduce the aerofoil's ability to generate lift as the flow separates from the surface at lower angles of attack.

Figure 19 presents a comparison between the performance of the optimal configurations for the S825, S818, and S826 aerofoils to determine which profile thickness derives the greatest benefit from the simultaneous blowing and suction CFJ technique. As shown in Figure 19, aerofoils with greater thickness exhibit the most significant improvements from the application of this technique, achieving substantial gains in aerodynamic efficiency and a marked reduction in drag coefficient compared to the base case. Notably, the profiles with the largest

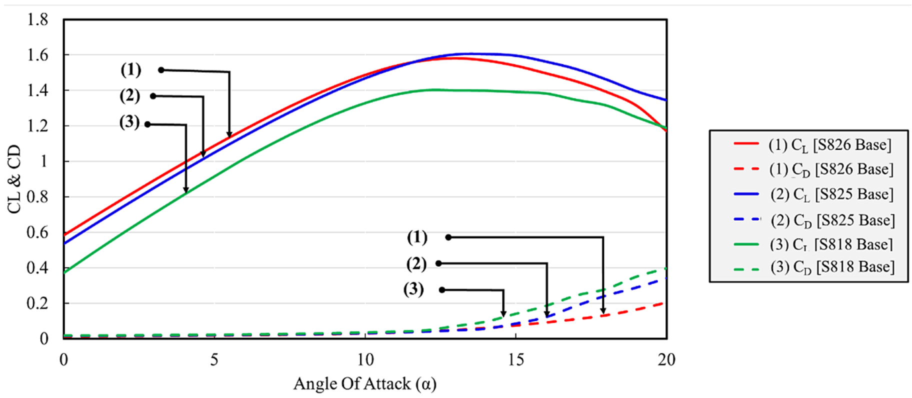

Figure 18. The variation of the lift and the drag coefficients over a range of angle of attack for different aerofoil thicknesses

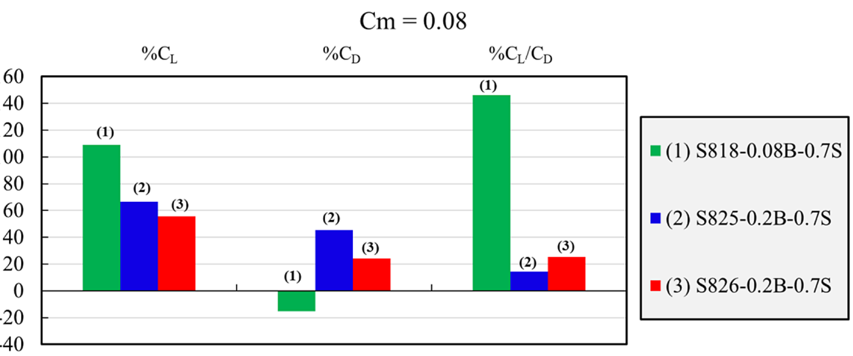

Figure 19. Influence of various thickness profiles with simultaneous blowing and suction CFJ technique at the onset stall angle of attack

thickness experience the highest rates of aerodynamic efficiency improvement. However, despite the high efficiency of the CFJ technique when applied to thicker profiles, this does not necessarily imply that it will yield the best results when used on turbine blades, particularly those with thick profiles located at the blade root. Future research will explore the impact of the CFJ technique's location on turbine blade performance and its potential to enhance the torque generated by wind turbines.

CONCLUSIONS

This study conducted CFD simulations to investigate the effects of the simultaneous blowing and suction Co-Flow Jet (CFJ) technique on the NREL S825, NREL S818, and NREL S826 aerofoils. The goal was to identify the most suitable configurations that would enhance the performance and assess the impact of profile thickness on the effectiveness of the CFJ technique. Various CFJ configurations, including 0.08B-0.7S, 0.08B-0.8S, 0.1B-0.7S, and 0.2B-0.7S, were tested for each aerofoil.

The simulations revealed that for the NREL S825, the S825-0.2B-0.7S configuration at $C_m = 0.08$ emerged as the best-performing configuration, showing a 66.38% increase in the lift coefficient. In addition, this possesses a 45.45% increase in the drag coefficient while achieving a 14.38% improvement in the lift-to-drag ratio. For the NREL S818, the S818-0.08B-0.7S configuration at $C_m = 0.08$ is proved to be the optimal choice, achieving a 109% increase in the lift coefficient, a 15.1% reduction in the drag coefficient, and a remarkable 146.18% enhancement in the lift-to-drag ratio. On the other hand, for the NREL S826, the S826-0.2B-0.7S configuration at $C_m = 0.08$ is found to be the most effective, with a 56% increase in the lift coefficient in addition to a 24% increase in the drag coefficient, and a 25% improvement in the lift-to-drag ratio.

The consistent success based on the C_m value of 0.08 across the best-performing configurations suggests that it is the most suitable momentum coefficient, among the configurations considered, for applying the CFJ technique to the NREL S-family aerofoils. Additionally, the study concluded that the CFJ technique is more effective with thicker aerofoils compared to high-lift aerofoils, indicating that thicker profiles are more conducive to aerodynamic improvements.

However, while the CFJ technique significantly enhances the aerodynamic properties of thicker profiles, its application to turbine blades, particularly at the root, may not yield the best results. Future research will explore the impact of CFJ technique location on turbine blade performance and its potential to enhance torque generation in wind turbines.

REFERENCES

1. Abbasi, S., Esmailzadeh Vali, S. 2022. Effects of simultaneous suction and blowing over an aerofoil on flow behavior and aerodynamic coefficients. Iranica Journal of Energy & Environment, 13(4), 424–432.
2. Arunraj, R., Logesh, K., Balaji, V., Ravichandran, T., Yuvashree, G.K. 2019. Experimental investigation of lift enhancement by suction-assisted delayed separation of the boundary layer on NACA 0012 aerofoil. International Journal of Ambient Energy, 40(3), 243–247.
3. Abul-Ela, S.M., Sayed, I.A., Elrefaie, E.M., Enhancing vertical-axis wind turbine self-starting with distinctive blade airfoil designs, Unpublished manuscript.
4. Balaji, K., Wessley, G J.J. 2020. Experimental investigations on the performance of a modified co-flow jet aerofoil. IJST, 13, 85.
5. Boling, J.S., Zha, G., Zeune, C. 2020. A high-speed, high-efficiency VTOL concept using coflow jet Aerofoil. In AIAA Aviation 2020 Forum 2792.
6. Bartl, J., Sagmo, K.F., Bracchi, T., Sætran, L. 2019. Performance of the NREL S826 aerofoil at low to moderate Reynolds numbers—A reference experiment for CFD models. European Journal of Mechanics-B/Fluids, 75, 180–192.
7. Elsakka, M.M., Ingham, D.B., Ma, L., Pourkashanian, M. 2021. Comparison of the computational fluid dynamics predictions of vertical axis wind turbine performance against detailed pressure measurements. International Journal of Renewable Energy Research, 11(1), 276–293.
8. Goodarzi, M., Fereidouni, R., Rahimi, M. 2012. Investigation of flow control over a NACA 0012 aerofoil by suction effect on aerodynamic characteristics. Canadian Journal on Mechanical Sciences & Engineering, 3(3), 102–109.
9. Ibrahim, M.G., Ibrahim, Z.A., Elrefaie, M.E. 2024. Investigation of static and dynamic behaviour of proportional flow control valve provided by pressure compensator. Journal of Al-Azhar University Engineering Sector, 19(72), 56–47.
10. James, S.E., Suryan, A., Sebastian, J.J., Mohan, A., Kim, H.D. 2018. Comparative study of boundary layer control around an ordinary aerofoil and a high

lift aerofoil with secondary blowing. Computers & Fluids, 164, 50–63.

11. Liu, J., Chen, R., You, Y., Shi, Z. 2022. Numerical investigation of dynamic stall suppression of rotor aerofoil via improved co-flow jet. Chinese Journal of Aeronautics, 35(3), 169–184.
12. Li, Y., Song, Q., Li, Q.S., Wang, D.L., Wu, X.P. 2021. Experimental investigation of wind loads on wind turbine blade under various turbulent flows. Advances in Structural Engineering, 24(16), 3809–3824.
13. Malcolm, D.J., Hansen, A.C. 2006. WindPACT Turbine Rotor Design Study: June 2000–June 2002 (Revised) (No. NREL/SR-500-32495). National Renewable Energy Lab.(NREL), Golden, CO (United States).
14. Müller-Vahl, H.F., Strangfeld, C., Nayeri, C.N., Paschereit, C.O., Greenblatt, D. 2015. Control of thick aerofoil, deep dynamic stall using steady blowing. AIAA journal, 53(2), 277–295.
15. Ren, Y., Zha, G. 2020. High efficiency integrated propeller-coflow jet aerofoil in cruise. In AIAA Scitech 2020 Forum 0787.
16. Sun, X., Xu, Y., Huang, D. 2019. Numerical simulation and research on improving aerodynamic performance of vertical axis wind turbine by co-flow jet. Journal of Renewable and Sustainable Energy, 11(1).
17. Tayebi, A., Torabi, F. 2024. Flow control techniques to improve the aerodynamic performance of Darrieus vertical axis wind turbines: A critical review. Journal of Wind Engineering and Industrial Aerodynamics, 252, 105820.
18. Wang, L., Alam, M.M., Rehman, S., Zhou, Y. 2022. Effects of blowing and suction jets on the aerodynamic performance of wind turbine aerofoil. Renewable Energy, 196, 52–64.
19. Xu, K., Zha, G. 2021, June. High efficiency wind turbine using co-flow jet active flow control. In Turbo Expo: Power for Land, Sea, and Air 84898, V001T40A003. American Society of Mechanical Engineers.
20. Xu, K., Zha, G. 2021, June. High efficiency wind turbine using co-flow jet active flow control. In Turbo Expo: Power for Land, Sea, and Air 84898, V001T40A003. American Society of Mechanical Engineers.
21. Xu, H.Y., Qiao, C.L., Ye, Z.Y. 2016. Dynamic stall control on the wind turbine aerofoil via a co-flow jet. Energies, 9(6), 429.
22. Yuan, R., Chen, R., Li, H., Yang, W., Li, X. 2023. Dynamic reliability evaluation and life prediction of transmission system of multi-performance degraded wind turbine. CMES-Computer Modeling in Engineering & Sciences, 135(3).
23. Yousefi, K., Saleh, R., Zahedi, P. 2014. Numerical study of blowing and suction slot geometry optimization on NACA 0012 airfoil. Journal of Mechanical Science and Technology, 28, 1297–1310.
24. Zha, G.C., Carroll, B.F., Paxton, C.D., Conley, C.A., Wells, A. 2007. High-performance aerofoil using coflow jet flow control. AIAA journal, 45(8), 2087–2090.
25. Zhang, S., Yang, X., Song, B. 2021. Numerical investigation of performance enhancement of the S809 aerofoil and phase VI wind turbine blade using co-flow jet technology. Energies, 14(21), 6933.
26. Zhu, C., Qiu, Y., Feng, Y., Wang, T., Li, H. 2022. Combined effect of passive vortex generators and leading-edge roughness on dynamic stall of the wind turbine aerofoil. Energy Conversion and Management, 251, 115015.